SCIENCE CHINA
Information Sciences

• RESEARCH PAPER •

July 2021, Vol. 64 172203:1–172203:18
https://doi.org/10.1007/s11432-020-2961-8

Event-triggered shared lateral control for safe-maneuver of intelligent vehicles

Yan JIANG, Xinglong ZHANG*, Xin XU, Xing ZHOU & Zhengzheng DONG

College of Intelligence Science and Technology, National University of Defense Technology, Changsha 410073*, China*

Received 2 January 2020/Revised 23 April 2020/Accepted 29 May 2020/Published online 18 May 2021

Abstract With the increasing number of cars, road traffic accidents have caused a lot of losses every year and human factors play an important role in many cases. Applying active safety assistance control or shared control techniques in intelligent vehicles is promising to reduce the number of traffic accidents. In this context, the dynamic optimization of the shared control policy and the smooth transitions of control authority between human drivers and intelligent driving systems are critical issues to be solved. Motivated by this, this paper proposes an event-triggered shared control approach for safe-maneuver of intelligent vehicles with online risk assessment. In the proposed approach, a Bayesian regularized artificial neural network (BRANN) is designed to predict vehicle trajectories and build a quantization function to assess the risk level owing to potential collision events. The shared controller dynamically optimizes the shared control policies between the human and the intelligent driving system via solving a model predictive control (MPC) problem. The predicted driving behaviors in the prediction horizon are pre-computed with a finite-horizon model predictor steering the predicted trajectories contributed by human driving. Moreover, smooth transitions back to human driving mode are realized via adding penalties on the shared control of the intelligent driving system. Three simulation scenarios in the PreScan environment, i.e., rear-end collision avoidance, lane-keeping and unskilled driving, are studied to test the effectiveness of the proposed approach. The simulation results, including the comparison with a linear quadratic regulator (LQR)-based shared controller, are reported, which show that the proposed approach can timely evaluate dangerous events and realize safe driving in terms of collision avoidance and lane-keeping. Also, the proposed approach outperforms the LQR-based shared controller in terms of smooth transitions.

Keywords trajectory prediction, risk assessment, shared lateral control, model predictive control

Citation Jiang Y, Zhang X L, Xu X, et al. Event-triggered shared lateral control for safe-maneuver of intelligent vehicles. Sci China Inf Sci, 2021, 64(7): 172203, https://doi.org/10.1007/s11432-020-2961-8

1 Introduction

Road traffic accidents caused great losses every year and the improper behaviors of human drivers are one of the main causes. In daily driving activities, human drivers may suffer unawareness of their vehicles in potential danger owing to fatigue, distraction or blind spots, or may fail to avoid collisions caused by faulty operation and poor driving skills. Intelligent vehicles are promising to achieve a safer and more efficient driving experience. For the past decades, the developments of techniques required for autonomous driving have made significant progress in areas including smart sensing, decision making and motion control. However, the reliability and robustness of autonomous driving vehicles cannot satisfy the requirements of complex traffic conditions. For this reason, the research area on human-machine coordination and shared control for advanced assistant driving has received special attention, see for instance [1,2]. Unlike autonomous driving, human-machine cooperative driving allows shared and switched control between humans and vehicles to realize driving tasks with the goal of reducing the driver's labor intensity and traffic accidents. There are three critical issues in the process of cooperative driving, including (i) when to start the cooperation, (ii) how to cooperate on driving tasks, and (iii) at what time the cooperation is over. Although each of these issues has been separately studied in previous studies, see for instance [1, 3–5],

* Corresponding author (email: zhangxinglong18@nudt.edu.cn)

© Science China Press and Springer-Verlag GmbH Germany, part of Springer Nature 2021

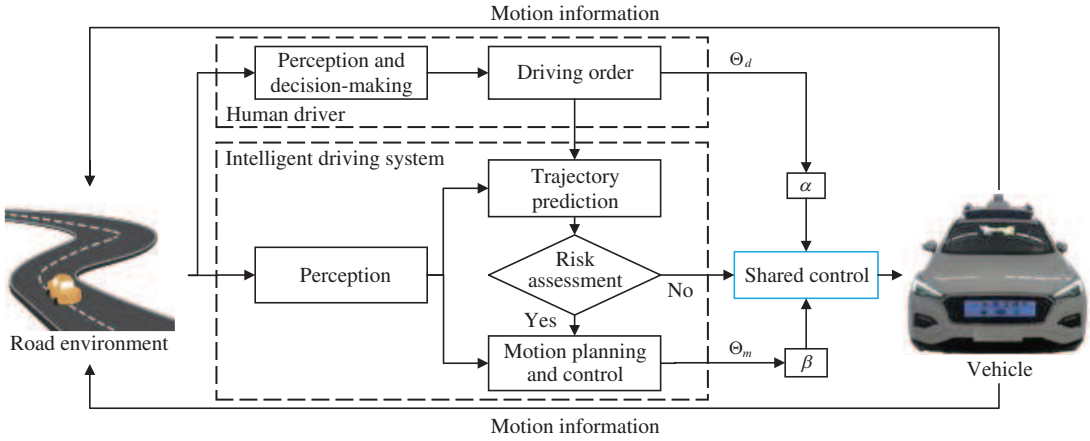

Figure 1 (Color online) Diagram of the shared control framework.

but the effectiveness is difficult to be validated as the above issues are mutually coupled. Few studies can offer realistic solutions with all the issues considered. In addition, the dynamic optimization of control authority between the intelligent system and the human has not been addressed in the existing studies, see [1,2]. Indeed, dynamically optimizing the switching of control authority can be very useful to enforce smooth and active transitions between the shared controller and human driving mode. Motivated by the above problems, this paper proposes an event-triggered human-machine shared control approach for collision-free maneuver. The main diagram of the proposed framework is depicted in Figure 1. Human driving orders can be applied to the driving system all the time, while the control contributed by the machine is triggered when a potential risk event is detected. In this case, the shared, final control action is the integration of the human and the machine and the shared controller is continuously optimized according to a safety-oriented performance index.

The contributions of this paper include the following three aspects. (i) We propose an online risk assessment algorithm making only use of historical driving information. This method avoids monitoring the driver's status directly. The main idea is to learn and predict the vehicle trajectory with past motion information of the vehicle by using a Bayesian regularized artificial neural network (BRANN). Then, the potential risk is quantized using the predicted trajectory and the detected environment. (ii) We design an event-triggered shared lateral controller for collision avoidance. The algorithm optimizes the shared control policy of the human driver and the machine dynamically according to a safe-driving oriented objective function. The driver's future behaviors used in the prediction horizon are pre-computed via modeling itself as an online model predictor steering the predicted trajectories contributed by human driving. Moreover, the smooth transition to the driver mode is realized via adding penalties on the shared control in the optimization problem. (iii) We test and compare the proposed controller with the linear quadratic regulator (LQR)-based shared controller described in [6] in three high-fidelity simulation examples, including rear-end collision avoidance, lane-keeping and unskilled driving, which shows smoother transitions and smaller intervention time period of the proposed approach than that of the LQR-based one.

The paper is organized as follows. Related work is primarily reviewed in Section 2. Section 3 introduces the linear time-varying vehicle model to be used and the control objective. In Section 4 the main idea of the risk assessment strategy is described. Section 5 gives the design details of the shared lateral controller, while simulation implementations and results are presented and collected in Section 6. Finally, concluding remarks are drawn in Section 7.

2 Related work

Among all the shared control strategies, many studies rely on driving models or the direct prediction of the driver's intention. In these studies, one line is to use switching control between the human and machine. For instance, a taking over controller has been proposed in [7] with a camera supervising the driver's intention. In [8] a switching controller has been developed, where a fault detection algorithm is used to detect the driver's abnormal steering behaviors. In case the failure occurs, the machine will take

over the control. As it has been noted in [9], there are potential safety issues caused by driver or machine factors in the process of control switching. Hence, the shared control of the driver and machine is of great importance. Shared controllers using physical-based driver models have been developed in [10–12]. In [13], a fuzzy logic-based sliding mode controller has been proposed to achieve shared control, and a vision-based measure system was used for predicting vehicle trajectories. From the theoretical perspective, a shared controller for linear constrained systems has been presented in [14], and extended in [15,16] taking into consideration of the effects of disturbances. The robustness property is guaranteed by resorting to Lyapunov arguments. A shared controller has been proposed in [17], where the stability in presence of uncertainty of driver model is discussed. A data-driven shared steering control algorithm with resorting to adaptive dynamic programming has been proposed in [18], where the input-to-state stability property is proven with small gain theory. In [19], a shared control design strategy from the driver's experience perspective has been presented to achieve good driving experience. Different from the aforementioned studies, the proposed approach in this paper does not rely on a physical-based driver model or directly measure the driver's intention. Instead, the driver's future behavior is modeled as an online model predictor steering the predicted trajectory contributed by the driver.

In authority allocation, a shared controller with fixed weights has been adopted in [20], where a predictive path planning method is used for lane-keeping and collision avoidance. In [21], the driver is assumed to be cooperative and the shared controller is trusted, and the effect of driver's adaptation is evaluated according to the weight variation of the machine. A framework based on model predictive control (MPC) has been formulated in [22] to perform trajectory planning, threat assessment, and collision avoidance. The control shares of the driver and controller are adjusted through threat assessment. However, factors caused by the driver are not taken into account. In [23], a semi-autonomous controller based on nonlinear MPC has been proposed. The approach utilizes a driving model to generate the driver's behavior in the prediction horizon and integrates the threat assessment into the constraints of the MPC controller. The objective of the controller is to provide minimal intervention without compromising safety. This mechanism ignores the feasibility of the prediction of driver's behaviors and fails to consider the quality of planned path and driver's acceptance of the controller. The main difference of our approach lies in the fact that the shares of control contributed by humans and machines can be explicitly optimized in the proposed approach. Recent contributions described in [24,25] have also shown the capability of MPC in solving path-following control problems of autonomous driving vehicles as well as other constrained and nonlinear control systems. In [26], an approximate dynamic programming (ADP)-based approach has been proposed to solve the human-machine shared control problem for robot arms. Indeed, ADP is an effective tool for solving adaptive control problems. However, in this paper an important perspective is to enforce dynamic optimization and active transitions of the control authority between the intelligent system and human driving under safety constraints. This might be difficult with ADP owing to the trial-and-error learning nature and to the approximate neural network adopted.

To better select the occasion to assist the driver, an automated system needs to predict the trajectory of the host vehicle and evaluate its safety online. Time-to-collision (TTC) is the earliest method utilized to judge the time to take evasive action to avoid a collision, see [27] for instance, which is the ratio of the distance from the host vehicle to the obstacle and the speed difference. According to [28], the distance can also be divided based on the variations of speeds and accelerations. The difficulty is that neither the method based on constant velocity nor constant acceleration can accurately predict the trajectory of the host vehicle, especially when there are varying maneuvers. A method to predict the future states of a vehicle has been proposed in [29]. This approach depends on precise vehicle models and deterministic driving behaviors. However, a realistic vehicle dynamical model is usually time-varying and the driver's behavior is probabilistic. In [30], two probabilistic algorithms have been proposed for measuring collision risk and predicting collision probability. The results reveal that Markov chain and Monte Carlo-based methods are applicable to estimate the subsequent maneuver and the maneuver time of collision avoidance system. One of the drawbacks of probabilistic methods is that they are computationally intensive. In this work, we propose a new quantization function for risk event assessment, according to which a simple triggering law is established.

In the viewpoint of collision avoidance, fruitful studies have been devoted to enforcing safety control in the human-machine shared framework. Among them, in [31], a constrained planning and control method for semi-autonomous vehicle collision avoidance has been proposed, which allows the operator to navigate freely within safe homotopies and introduces control actions when necessary. Different from the idea of minimally-invasive control in [31], an MPC algorithm that considers the constraints on the

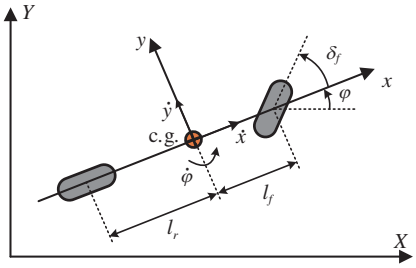

Figure 2 (Color online) The simplified "bicycle" model: c.g. is the center of gravity of the vehicle, x and y are the longitudinal and lateral positions of the vehicle in the body-fixed coordinates, respectively, X and Y are positions in the global coordinates, respectively, φ is the vehicle yaw angle, δ_f is the steering angle for the front wheel, l_f and l_r are the distance from the front and rear axles to c.g., respectively.

front wheel steering angle and the lateral tire force has been proposed in [32] for tracking a time-varying desired path. In addition to the aspect of dealing with constraints, adjusting the force in human-machine interaction process is another important way to avoid collisions. In [33], a joystick impedance control method has been proposed for semi-autonomous obstacle avoidance of unidirectional wheelchair. In [34], a haptic steering direction guidance system for pedestrian-vehicle collision avoidance has been discussed. Relying on the prediction of the future intervention time, a haptic steering feedback approach has been proposed in [35], where the trade-off between following the driver's action and steering a reference path is considered. It is highlighted that the implementation of haptic shared control requires additional motors and controllers to the steering wheel and gas pedal to interact with human drivers in real-time, which increases the complexity of the system. Differently, the method proposed in this paper belongs to indirect shared control, which is easy to implement on vehicles using X-by-wire control technology.

3 Linear time-varying vehicle model and control objective

In this section, we first present the linear time-varying version of the lateral vehicle model, and then introduce the human-machine shared control objective.

3.1 Linear time-varying vehicle model

As we are interested in the lateral control methods of passenger vehicles, in line with [36, 37], a bicycle model of the lateral vehicle dynamics is considered, which is illustrated in Figure 2.

Based on the assumptions of small front wheel steering angles and a linear tire model, as presented in [37], the differential equations of vehicle dynamics for a vehicle with a constant longitudinal speed can be written as

$$\begin{aligned}
&m\ddot{y} = -m\dot{x}\dot{\varphi} + 2\left[C_{cf}\left(\delta_f - \frac{\dot{y} + l_f\dot{\varphi}}{\dot{x}}\right) + C_{cr}\frac{l_r\dot{\varphi} - \dot{y}}{\dot{x}}\right],\\
&m\ddot{x} = 0,\\
&I_z\ddot{\varphi} = 2\left[l_fC_{cf}\left(\delta_f - \frac{\dot{y} + l_f\dot{\varphi}}{\dot{x}}\right) - l_rC_{cr}\frac{l_r\dot{\varphi} - \dot{y}}{\dot{x}}\right],\\
&\dot{Y} = \dot{x}\sin\varphi + \dot{y}\cos\varphi,\\
&\dot{X} = \dot{x}\cos\varphi - \dot{y}\sin\varphi,
\end{aligned} \tag{1}$$

where m is the mass of the vehicle, C_{cf} and C_{cr} are the cornering stiffness of the front and rear tires, respectively, I_z is the yaw moment of inertia. The mapping of the front wheel angle δ_f and the steering wheel angle Θ is simplified to $\delta_f = \Theta/\gamma$, where γ is the steering ratio. Let $\xi = [\dot{y}, \dot{x}, \varphi, \dot{\varphi}, Y, X]^{\mathrm{T}}$ and $u = \Theta$ denote the state and input, respectively, and to reduce the online computational load, system (1) is discretized with a sampling interval T, and written as

$$\xi(k+1) = A(k)\xi(k) + B(k)u(k), \quad \eta(k) = C\xi(k), \tag{2}$$

where k is the discrete-time index, $\xi(k)$ and $u(k)$ represent the current state and input information, respectively, $\xi(k+1)$ is the successive state at the next sampling time, $\eta(k)$ is the output which consists

of the global position Y and the yaw angle φ, and

$$A=\begin{bmatrix} a_{11} & a_{12} & 0 & a_{14} & 0 & 0 \\ 0 & 1 & 0 & 0 & 0 & 0 \\ 0 & 0 & 1 & T & 0 & 0 \\ a_{41} & a_{42} & 0 & a_{44} & 0 & 0 \\ a_{51} & a_{52} & a_{53} & 0 & 1 & 0 \\ a_{61} & a_{62} & a_{63} & 0 & 0 & 1 \end{bmatrix}, \quad B=\begin{bmatrix} b_1 \\ 0 \\ 0 \\ b_4 \\ 0 \\ 0 \end{bmatrix}, \quad C=\begin{bmatrix} 0 & 0 & 1 & 0 & 0 & 0 \\ 0 & 0 & 0 & 0 & 1 & 0 \end{bmatrix},$$

where $a_{11}=1+T\frac{-2(C_{cf}+C_{cr})}{m\dot{x}}$, $a_{12}=T(\frac{2C_{cf}(\dot{y}+l_f\dot{\varphi})+2C_{cr}(\dot{y}-l_r\dot{\varphi})}{m\dot{x}^2}-\dot{\varphi})$, $a_{14}=T(-\dot{x}+\frac{2(l_rC_{cr}-l_fC_{cf})}{m\dot{x}})$, $a_{41}=T\frac{2(l_rC_{cr}-l_fC_{cf})}{I_z\dot{x}}$, $a_{42}=T\frac{2l_fC_{cf}(\dot{y}+l_f\dot{\varphi})-2l_rC_{cr}(\dot{y}-l_r\dot{\varphi})}{I_z\dot{x}^2}$, $a_{44}=1+T\frac{-2({l_f}^2C_{cf}+{l_r}^2C_{cr})}{I_z\dot{x}}$, $a_{51}=T\cos\varphi$, $a_{52}=T\sin\varphi$, $a_{53}=T(\dot{x}\cos\varphi-\dot{y}\sin\varphi)$, $a_{61}=-T\sin\varphi$, $a_{62}=T\cos\varphi$, $a_{63}=-T(\dot{y}\cos\varphi+\dot{x}\sin\varphi)$, $b_1=T\frac{2C_{cf}}{m\gamma}$, $b_4=T\frac{2l_fC_{cf}}{\gamma I_z}$.

3.2 Control objective

The control objective considered is to design an event-triggered shared controller to assist drivers for safe maneuver in case potentially dangerous events occur. Along the line with [21], we propose an indirect shared control integration to be applied to the steering-by-wire system of the vehicle as

$$u=\alpha\Theta_d+\beta\Theta_m, \tag{3}$$

where Θ_d and Θ_m are the steering wheel angles derived from the driver and intelligent system, respectively, $\alpha\in[0,1]$ and $\beta\in[0,1]$ are the shares of the efforts by the human and intelligent system, satisfying

$$\alpha+\beta=1, \tag{4}$$

where $\alpha=0$ means the vehicle is in fully autonomous driving mode, while $\beta=0$ corresponds to only human taking over the vehicle. α and β are regarded as decisive variables in the finite-horizon optimization problems later described.

Remark 1. Different from the work in [21] where α and β are set as constants, the advantage of the design in our paper is that the control shares of the driver and intelligent system can be explicitly expressed and be continuously optimized, which is fundamental to achieve smooth transitions between shared control and human driving.

4 Collision risk assessment

In this section, we present the trajectory prediction and collision detection of the host vehicle to determine the timing for intervention and the limit of the share of the driver.

4.1 Trajectory prediction

In the shared control framework, the prediction of future trajectory evolution is necessary for risk assessment and collision avoidance control. One way to achieve this is to analyze and predict the driver's actions to be applied to the vehicle dynamic model in order to compute the trajectory of the vehicle, see [7,38]. However, this might lead to inaccuracy of the prediction as subjective human driving shows strong uncertainty. Directly predicting the vehicle trajectory with past maneuver information is advisable in this case. As described in [39], traditional physical-based motion prediction methods utilize dynamic and kinematic models to predict future trajectories. There are usually two common models adopted, the constant velocity and constant acceleration ones. Approaches with the above models perform well when the driving behavior changes slowly, for instance in the case of lane-keeping. However, they have obvious deadlocks when the driving behavior varies continuously. Hence, the performance is only satisfactory for short-term prediction. Learning-based algorithms such as recurrent neural networks in [40] and dynamic Bayesian networks in [41] have been developed to achieve long-term prediction and even interaction with the environment.

Along the same line, we design the BRANN to learn the lateral errors between predicted trajectories and real trajectories. The idea of using Bayesian regularization for curve interpolation was firstly proposed in [42]. Recent studies using BRANN have been proposed for predicting complex models with noises, see [43, 44], which shows its capability in reducing the possibility for overfitting and improving the prediction quality and generalization. The prediction of vehicle trajectory is a similar problem and nontrivial task owing to the existence of uncertainties caused by human driving and the surrounding environment and to the requirement of reliable prediction results that is to be used in the shared controller. Hence, we propose for the first time to use the BRANN with a single hidden layer for learning and predicting vehicle trajectory with past vehicle information. The network is trained with a training set of inputs and targets in the form $\{\phi_1, e_1\}, \{\phi_2, e_2\}, \ldots, \{\phi_N, e_N\}$, where N is the number of data samples, for $i = 1, \ldots, N$, $e_i \in \mathbb{R}^l$ is a vector of the future values of lateral errors, while the corresponding $\phi_i \in \mathbb{R}^{2n}$ contains the past n steps of information of steering wheel angles and velocities. Assuming that the targets are generated by $e_i = g(\phi_i) + \varepsilon_i$, where $g(\phi_i)$ is an unknown function approximated by the network and ε_i is an independent Gaussian noise. The objective is to minimize the following regularized cost function, i.e.,

$$V = \gamma_1 \sum_{i=1}^{N} \|e_i - f(\phi_i)\|^2 + \gamma_2 \left(\sum_{i=1}^{l} \|\mathrm{col}_i\{W_b\}\|^2 + \|b\|^2 \right), \tag{5}$$

where the first term is the sum of squared errors, the second term is the regularization term, $\gamma_1 > 0$ and $\gamma_2 > 0$ are regularization parameters, $f(\phi_i) = W_b^{\mathrm{T}} h(\phi_i) + b$, $W_b \in \mathbb{R}^{p \times l}$. The optimization problem with cost (5) is trained in the framework of Bayesian learning. Specifically, we utilize David MacKay's Bayesian techniques and the Gauss-Newton approximation described in [45] to train the network, while the implementing details are neglected for space limitations.

Note that, different from the simplified dynamical model (2), we add steering wheel velocity as one of the inputs in order to capture the precise variation of lateral errors. In the online test process, at any time instant, the steering wheel angles and steering wheel angular velocities in the last n time steps are used as the input variables to be applied to the neural network to compute the future lateral prediction errors in the next l time steps.

The data sets used for training and testing the neural network are collected in a driving simulator, which will be described in detail in Section 6. Figure 3 shows the predicted trajectories of the host vehicle in a lane change process obtained by the physical-based methods with constant velocity and acceleration respectively and the proposed approach. It can be seen from Figures 3(a) and (b) that the trajectories predicted by the method using the constant velocity model cannot reflect the change of vehicle's acceleration, while the trajectories predicted by that with the constant acceleration model perform better. It can be seen in Figure 3(c) that the trajectory of the host vehicle can be accurately predicted with the proposed method even in a longer prediction horizon.

To better show the performance of the proposed trajectory prediction approach, the mean square errors (MSE) computed in the training and testing processes are collected and shown in Figure 4. The MSE is 0.53 at the 12th epoch, which is the terminating point where the MSE stops decreasing. Also, it can be shown in Figure 5 that the gap between the training and testing is small, which reveals the generalization capability of the proposed approach.

4.2 Collision detection

When a potential risk occurs, it is crucial to intervene at an appropriate time instant. This requires the detection of future collisions with resorting to the predicted trajectory computed. In the following, we introduce the main idea to perform future collision prediction, and then define the intervention time according to the risk evaluation. To simplify the problem, it is assumed that all the dynamic obstacles in the environment move at a constant speed. Also, the positions and velocities of the obstacles can be measured by on-board sensors in real-time.

In principle, it is advisable to regard the vehicle as a point and reformulate the environment using the configuration space concept. However, as the shape of vehicle is rectangular, it is difficult to perform exact transformation in configuration space. For this reason, along the line with [37], we use the circumradius of the vehicle to expand the size of obstacles in longitudinal direction and use 0.6 times the width of the vehicle to expand the size of obstacles in lateral direction and to shrink the size of road boundaries. The main idea is shown in Figure 6.

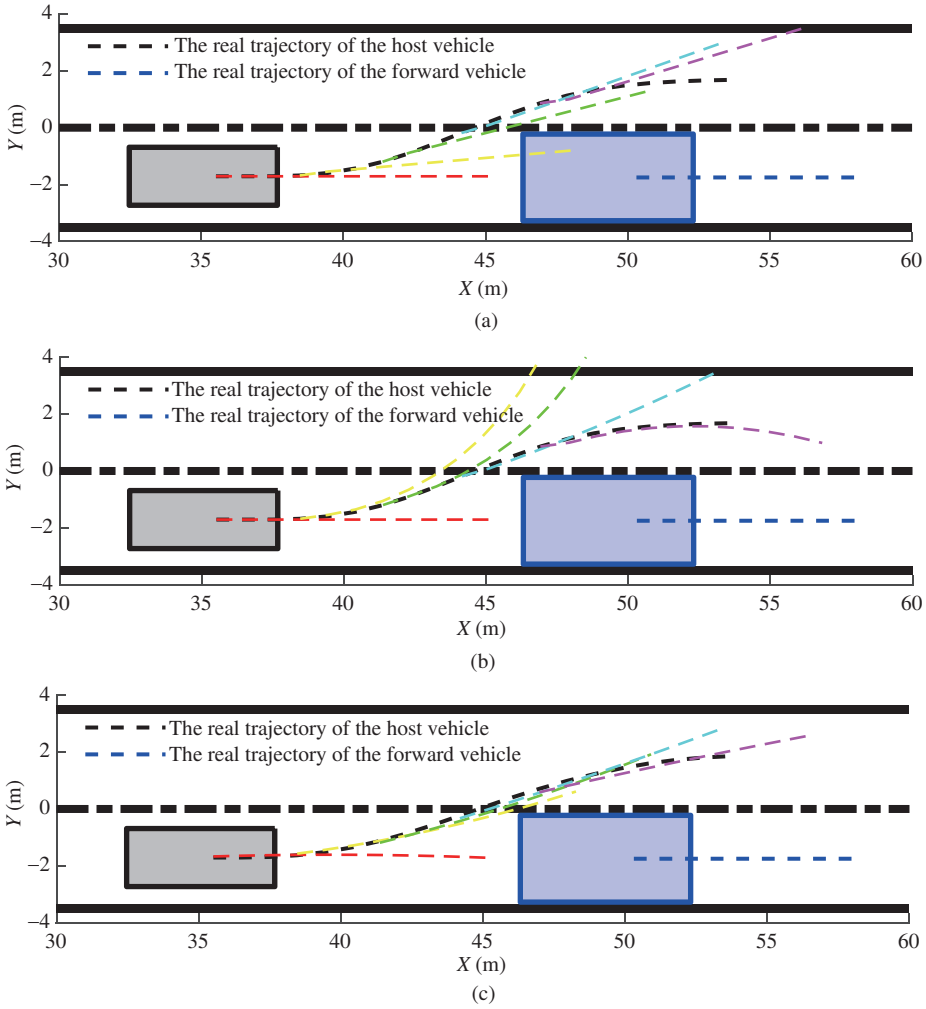

Figure 3 (Color online) The predicted trajectories of the host vehicle in a lane change process based on three different methods. (a) The constant velocity model; (b) the constant acceleration model; (c) the proposed method. The solid black and dash-dotted black lines represent the curbs and center-lines of roads, respectively. The solid black and blue rectangles represent the host and forward vehicles at a generic discrete-time sampling instant k_0, respectively. The dashed red, yellow, green, cyan and magenta lines represent the predicted trajectories of the host vehicle from k_0 to $k_0+3, k_0+6, k_0+9, k_0+12$, respectively.

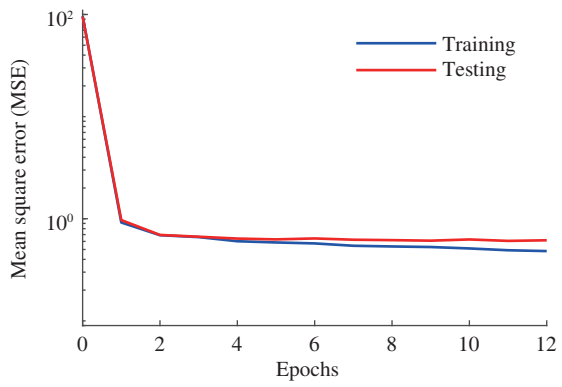

Figure 4 (Color online) Training and testing performance of the Bayesian regularized artificial neural network.

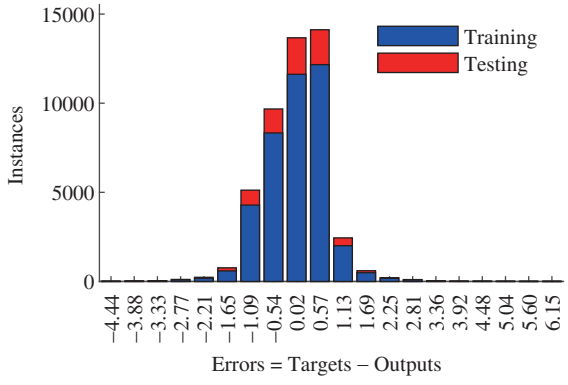

Figure 5 (Color online) The error distribution of the training and testing results at the 12th epoch.

With this design, it is ready to detect collisions using predicted trajectories. Consider the trajectory series $(x_1, y_1), \ldots, (x_{N_p}, y_{N_p})$, where N_p is the prediction horizon. We say a potential collision is detected

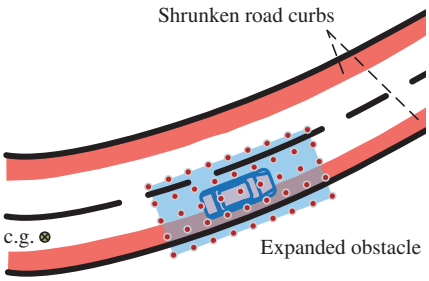

Figure 6 (Color online) The schematic diagram of the simplified collision detection. The red-filled strips and blue-filled rectangle represent the shrunken road curbs and expanded obstacle, respectively. The red dots represent the positions evenly chosen from the expanded obstacle in obstacle avoidance.

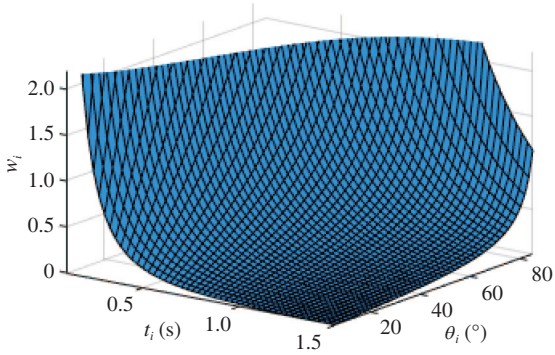

Figure 7 (Color online) The 3D surface graph of the risk assessment function.

if there exists a number $i = 1, \ldots, N_p$ such that

$$(x_i, y_i) \cap \Omega \neq \emptyset, \tag{6}$$

where Ω represents the set of obstacles.

Let I_i, $i = 1, \ldots, N_p$ denote an indicator function, which is given as follows:

$$I_i = \begin{cases} 1, & \text{for } (x_i, y_i) \cap \Omega \neq \emptyset, \\ 0, & \text{otherwise.} \end{cases}$$

Now, we propose a risk assessment function as

$$w = \sum_{i=1}^{N_p} I_i w_i, \tag{7}$$

where $w_i = \frac{\tan\theta_i}{e^{t_i} t_i^2}$, $\theta_i \in [0, \pi/2]$ is the difference between the heading angle of the host vehicle and the tangential direction angle of the curb or obstacle boundary at the i-th time step, and $t_i > 0$ is the predicted time corresponding to the predicted trajectories such that $t_i = iT$. The variations of w_i in three-dimension with respect to t_i and θ_i are shown in Figure 7, which shows that the smaller t_i or the larger θ_i, the larger w_i. Given a constant value w_0, if w is greater than w_0, we consider that the driver cannot guarantee safe driving, hence intervention is required, i.e., the shared lateral controller is triggered. To ensure safety in shared control mode, the share of control effort by human is limited, i.e.,

$$\alpha \leqslant \alpha_{\max}, \tag{8}$$

where

$$\begin{cases} \alpha_{\max} = 1, & \text{for } w < w_0, \\ \alpha_{\max} = \dfrac{w_0}{\ln w + w_0}, & \text{otherwise,} \end{cases}$$

where the value of w_0 is chosen by experience, here we set $w_0 = 1$. Figure 8 shows a specific example of the risk assessment result in a frontal collision scenario. The risk of a collision is detected as long as Eq. (6) is verified. In this case, the value of θ_i is close to $\pi/2$, which means the shared controller can be triggered immediately. Otherwise, as seen in Figure 8(b), if no intervention is allowed, a collision event will finally occur. The proposed risk assessment method can be also suitable for detecting a side collision, as shown in Figure 9. In this case, the value of θ_i can be smaller compared to the previous case, which means the value of w might be much smaller. This will lead to the intervention time much later, which is exactly the case in the side collision scenario. In this way, frequent interventions can be avoided, this is the advantageous point compared with the TTC method.

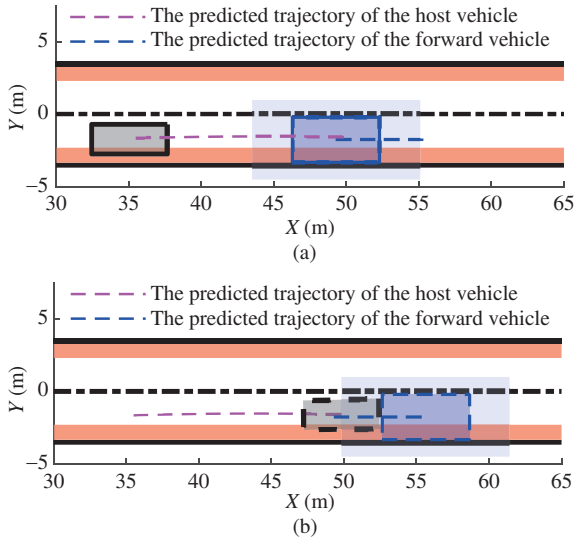

Figure 8 (Color online) The risk assessment for a frontal collision ($t_c = 1.5$ s, $w = 36.63$, $\alpha_{\max} = 0.22$), where t_c is the collision time starting from the current time instant. (a) The host and forward vehicles at a current time $t_0 = 0$: the solid black and solid blue rectangles represent the host and forward vehicles, respectively. (b) The host and forward vehicles at the collision time: the dashed black and dashed blue rectangles respectively represent the host and forward vehicles at the collision time.

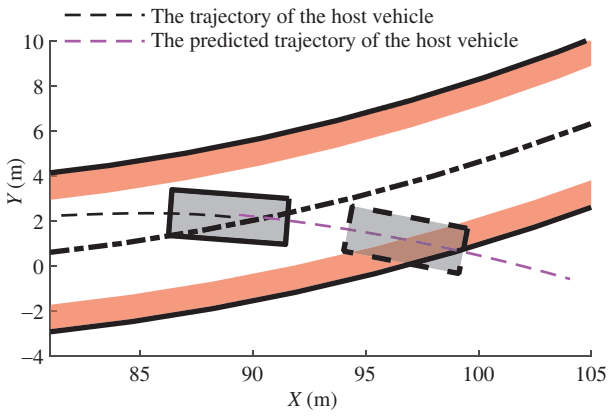

Figure 9 (Color online) The risk assessment for a side collision ($t_c = 0.8$ s, $w = 1.38$, $\alpha_{\max} = 0.76$). The solid black and dashed black rectangles respectively represent the host vehicle at the current and collision time.

5 Risk event-triggered shared lateral control

In this section, we firstly describe the prediction of driver's behaviors using the predicted future trajectory contributed by the driver. Then the main algorithm, the smooth transition strategy, as well as the implementation steps of the event-triggered shared lateral control are introduced.

5.1 Prediction of driver's behaviors

As it has been noted in [12, 17, 46], the driver's behaviors can be very useful for improving control performance, especially in a predictive control framework. To predict the driver's behaviors, in this paper, we utilize the predicted trajectory of the host vehicle to obtain the input intention of the driver via solving an MPC optimization problem. The main idea is to model the human driver's action as a model predictor.

The predicted trajectory is regarded as the reference to be followed, which is denoted as η_r. Note that, as in the shared control mode the predicted trajectory of the host vehicle is resulted by the integrated control action from the human and the intelligent driving system. In this special case, only the driver's past action information is used as the input of the trained BRANN algorithm to generate the corresponding trajectory prediction η_r. At any time instant k, considering $\overrightarrow{u}(k : k + N_c - 1) = u(k), \ldots, u(k + N_c - 1)$ as the future control sequence, the following optimization problem can be stated:

$$\min_{\overrightarrow{u}(k:k+N_c-1)} \sum_{j=1}^{N_p-1} \|\eta(k+j) - \eta_r(k+j)\|^2_{Q_\eta} + \sum_{j=0}^{N_c-1} (\|u(k+j)\|^2_{Q_\Theta} + \|u(k+j) - u(k+j-1)\|^2_R) \quad (9)$$

$$\text{s.t.} \quad \text{dynamics (2)},$$
$$\Theta_{\min} < u(k+j) < \Theta_{\max}, \ j = 0, \ldots, N_c - 1,$$

where N_p is the prediction horizon, $N_c \leqslant N_p$ is the control horizon, Q_η, Q_Θ, and R are positive-definite tuning matrices, $\Theta_{\min}$ and $\Theta_{\max}$ are the lower and upper bounds of the steering wheel angle, respectively. In optimization problem (9), the first item of the objective function is to minimize the errors between

the reference and the predictive trajectories generated by the vehicle dynamics model. In the second item, $\|u(k+j)\|^2_{Q_\Theta}$ is to optimize the amplitude of the steering action, which devotes to minimizing the energy input required by the human driver. The third item $\|u(k+j)-u(k+j-1)\|^2_R$ is to minimize the increment of the steering action, which is used for generating smooth driving behaviors.

At any time instant k, assume the optimal solution of (9) can be computed, that is $\overrightarrow{u}(k:k+N_c-1|k)$. Then the predicted driving behavior is given as

$$\Theta_d(k+j)=\begin{cases} u(k+j|k), & \text{for } j\leqslant N_c-1,\\ u(k+N_c-1|k), & \text{otherwise.}\end{cases} \tag{10}$$

5.2 Design of the shared lateral controller

Assume at a generic time instant t, a potential risk is detected, i.e., $w\geqslant w_0$, the shared lateral controller is activated. This requires to solve an online MPC optimization problem stated as follows:

$$\min_{\alpha,\beta,\overrightarrow{u}(t:t+N_c-1)} J(\xi(t),\overrightarrow{u}(t:t+N_c-1)), \tag{11}$$

$$\begin{aligned}\text{s.t.}\quad & \text{dynamics (2)},\\ & \text{constraints, (3), (4), (8), (10)},\\ & \Theta_{\min}<u(t+j)<\Theta_{\max},\ j=0,\dots,N_c-1,\\ & 0\leqslant\alpha\leqslant\alpha_{\max},\\ & 0\leqslant\beta\leqslant 1,\end{aligned}$$

where

$$J(\xi(t),\overrightarrow{u}(t:t+N_c-1))=\sum_{j=0}^{N_p-1}(\|\eta(t+j)-\eta_{\text{ref}}(t+j)\|^2_{Q_\eta}+J_{\text{obs}}(t+j))+\sum_{j=0}^{N_c-1}\|u(t+j)-u(t+j-1)\|^2_R,$$

η_{ref} is the reference path generated by a pre-assumed path planning module of the automated system, the input u in this case is the integration of the human behavior and the control action of the intelligent system. In (11), the first optimizing item minimizes the errors between reference and predictive trajectories. J_{obs} in the second item is a soft barrier function for obstacle avoidance, which is defined as

$$J_{\text{obs}}(t+j)=\sum_{i=1}^{M}\frac{S_{\text{obs}}}{(X(t+j)-X_i^o(t+j))^2+(Y(t+j)-Y_i^o(t+j))^2+\epsilon},$$

where (X_i^o,Y_i^o), $i=1,\dots,M$ are the positions evenly chosen from the set of expanded obstacles (as shown in Figure 6), M is the number of points adopted, $S_{\text{obs}}>0$ is a weighting coefficient, and $\epsilon>0$ is a small positive scalar to ensure the denominator being not zero. Similar to that of (9), the third term is to generate smooth shared control actions for the vehicle.

At any time instant t, assume the optimal solution of (11) is computed as $\overrightarrow{u}(t:t+N_c-1|t)$. At the current time t, the control action to be applied to the system (2) is $u(t|t)$. Then at the subsequent time instant $t+1$, the optimization problem (11) is solved repeatedly according to the receding horizon strategy.

Remark 2. The stability of the shared controller can be verified under mild assumptions. First note that the future reference trajectory ξ_{ref} can be known from the motion planning module. Hence, it is possible to write (2) with coordinate transformation, i.e., $e(k)=\bar{A}(k)e(k)+\bar{B}(k)u(k)+d, e_\eta(k)=\bar{C}(k)e(k)$, where $e=\xi(k+1)-\xi_{\text{ref}}$, $e_\eta=\eta-\eta_{\text{ref}}$, $\bar{A}(k)$, $\bar{B}(k)$, and $\bar{C}(k)$ can be computed according to [36], d is a function of the yaw rate. It is assumed d is (nearly) constant. Then the pair $(e_{\eta,s},\delta u_s)=(0,0)$ is the origin of the incremental version of the transformed model, where $\delta u(k)=u(k)-u(k-1)$. Assume that $N_p=N_c$, $S_{\text{obs}}\to 0$, $N_p\to+\infty$, and there exists a feedback gain K such that $F(k)=\bar{A}(k)+\bar{B}(k)K$ is Schur stable, and then the cost function in (11) can be rewritten as $J=\sum_{j=0}^{\bar{N}_p-1}(\|e_\eta(t+j)\|^2_{Q_\eta}+\|\delta u(t+j)\|^2_R)+\|e_\eta(t+\bar{N}_p)\|^2_P$, where $P=\sum_{j=0}^{+\infty}((F(k)^j)^{\mathrm{T}}Q_\eta F(k)^j+K^{\mathrm{T}}RK)$, $\bar{N}_p<N_p$ is sufficiently large. In this case, Eq. (11) is equivalent to a quasi-infinite MPC problem. Hence the stability can be guaranteed according to [47, 48].

5.3 Smooth transitions to human driving

The transition from shared control to human driving mode is one of the difficult issues in human-machine cooperative driving. In the transition process, safety and smoothness are the two factors to be considered. For this reason, the transition is activated if the following conditions are satisfied: (i) the risk level $w < w_0$; (ii) the past shares of human behaviors $\alpha(t-i) \geqslant \bar{\alpha}$, for $i = 1, \ldots, r$, where r is a positive number and $\bar{\alpha} > 0$ is the threshold value. The first condition can be easily verified as long as there is no potential frontal risk. But the second condition is not guaranteed to be satisfied by (11). Hence, we propose an optimization-based approach to enforce this. We simply add two more terms in the objective function of (11), i.e.,

$$\bar{J} = J + \varepsilon_1 \beta + \varepsilon_2 (\beta - \beta_{\text{pre}})^2, \tag{12}$$

where β_{pre} is the share of the intelligent system in the previous time instant. The item $\varepsilon_1 \beta$ is added to enforce $\beta \to 0$ such that a safe smooth transition from the shared control mode to human driving mode can be achieved. The last term is to penalize the deviation between the previous and current share of the intelligent system, which can be beneficial for achieving smooth motion trajectories. The objective function $\bar{J}$ is used instead of J in (11) if no potential risk is detected. That is to say, the weighting scalars ε_1, ε_2 are chosen as

$$(\varepsilon_1, \varepsilon_2) = \begin{cases} 0, & \text{for } w \geqslant w_0, \\ (\bar{\varepsilon}_1, \bar{\varepsilon}_2), & \text{otherwise}, \end{cases}$$

where $\bar{\varepsilon}_1$ and $\bar{\varepsilon}_2$ are tuning parameters.

5.4 Implementation of the event-triggered shared control algorithm

The main implementation steps of the event-triggered shared lateral control are described in Algorithm 1. Some remarks on the implementation of the proposed shared controller are in order, i.e., some trade-offs are highlighted.

- The first trade-off is between control performance and real-time property: large values of N_p and N_c might be chosen to improve the control performance, but with an increasing computational burden.
- The second one is between tracking performance and collision avoidance: a suitable value of S_{obs} is advisable to ensure safe collision avoidance, without degrading the tracking performance.
- The last one is between fast and smooth transitions: setting $\bar{\varepsilon}_1$ larger than $\bar{\varepsilon}_2$ will enforce fast switches from the shared control to human driving mode, but might lead to non-smooth transitions.

Algorithm 1 Implementation steps of the event-triggered shared lateral control

Require: set tuning parameters Q_η, Q_Θ, R, S_{obs}, $\bar{\varepsilon}_1$, $\bar{\varepsilon}_2$, N_p, N_c, $\bar{\alpha}$, r;
for $k = 1, \ldots$ **do**
  Generate $\eta_r(k+1), \ldots, \eta_r(k+N_p)$ using BRANN algorithm;
  Compute the risk level w with (7);
  if $w < w_0$ **then**
    Remain in human driving mode;
  else
    Obtain $\Theta_d(k+1), \ldots, \Theta_d(k+N_p-1)$ with (9);
    Compute the shared control action $u(k|k)$ with the shared controller (11);
    Apply $u(k|k)$ to the vehicle;
    if $w < w_0$ **then**
      Compute $u(k|k)$ with the shared controller (11) using cost (12);
      Apply $u(k|k)$ to the vehicle;
      if $\alpha(k-i) \geqslant \bar{\alpha}$, $i = 1, \ldots, r$ **then**
        Break and switch back to human driving mode;
      end if
    end if
  end if
end for

6 Simulation studies

In this section the event-triggered human-machine cooperative shared lateral control system was tested on a driving simulator in the PreScan environment for collision-free maneuver in the following three typical

Table 1 The value of the parameters

Parameter	Value	Unit	Parameter	Value	Unit
m	1820	kg	Q_η	200	–
l_f	1.170	m	Q_Θ	100	–
l_r	1.770	m	R	10000	–
C_{cf}	72653	N/rad	S_{obs}	10	–
C_{cr}	121449	N/rad	M	45	–
I_z	3746	kg·m^2	$\bar{\alpha}$	0.8	–
$\Theta_{\min}$	-450	$^\circ$	r	5	–
$\Theta_{\max}$	450	$^\circ$	$\bar{\varepsilon}_1$	50	–
γ	20	–	$\bar{\varepsilon}_2$	10	–
n	10	–	N	3147	–
p	100	–	κ	0.005	–
l	15	–			

scenarios: (i) rear-end collision on a straight-road caused by the driver's distraction; (ii) lane-departure on a curved road owing to wrong driving behaviors; (iii) assistance driving for unskilled drivers. For comparison, a shared lateral controller with the LQR described in [6] was considered. The control share of the human is given as

$$\alpha = \exp\left(-\frac{e_L^2}{\kappa^2}\right),$$

where e_L is the lateral error with respect to desired path and κ is a tuning parameter. The linear error model in [36] is used, where the input is the front wheel angle δ_f, while the state is $\zeta = [e_L, \dot{e}_L, e_H, \dot{e}_H]^{\mathrm{T}}$, and where e_H is the heading error with respect to the desired path.

6.1 Driving simulator

In order to test the proposed algorithm, we built a two-lane one-way road in the PreScan environment, as shown in Figure 10. The simulated road consists of several straight roads and curves covering the considered three scenarios. To perform real-time simulation, a simulation framework using Simulink (in MATLAB R2019a) and PreScan was established, and all the experiments were run on a computer with 3.2 GHz Intel Core i7 processor and 16 GB 3200 MHz DDR4 RAM. In addition, the training and testing processes of the BRANN were implemented using deep learning toolbox of MATLAB. In the experiments, human drivers interact with the simulation environment through a LogitechG29 steering wheel. The parameters γ_1 and γ_2 in the BRANN were initialized with $\gamma_1 = 1$ and $\gamma_2 = 0$, and the network weights W_b and biases b were initialized using the Nguyen Widrow method. At each iterative step, the Levenberg-Marquardt algorithm was used to compute the update of network weights and via minimizing (5). Then the parameters γ_1 and γ_2 were updated via estimating the posterior probability with the computed network weights and biases. The optimization problem (9) in each prediction horizon was solved with the Quadprog solver, while Eqs. (11) and (12) that contain nonlinear terms in the objective function were solved using the fmincon solver with an interior-point algorithm.

The parameters of the vehicle model used in this study were chosen as the same as the Audi A8 Sedan model provided by the PreScan software. The prediction and control horizon were selected as $N_p = 15$ and $N_c = 5$, the sampling time was chosen as $T = 0.1$ s. The velocity of the vehicle is relatively fixed at 10 m/s (36 km/h), which is a normal speed for urban road. To improve readability, the values of the parameters used in the controller are listed in Table 1.

6.2 Rear-end collision avoidance

In principle, driving on a straight road is an easy task. However, drivers might be distracted from the road owing to talking on the phone and texting messages. This might lead to obstacle detection failure and collision. We first tested our shared control method in this scenario. As shown in Figure 11, suppose that the host vehicle is driving along a straight road and the distracted driver fails to perceive the front truck that the driver is approaching.

Fortunately, the risk assessment module continuously predicts the trajectory of the host vehicle and evaluates its hazard level. When the risk value surpasses the threshold, i.e., $w \geqslant w_0$, the shared lateral

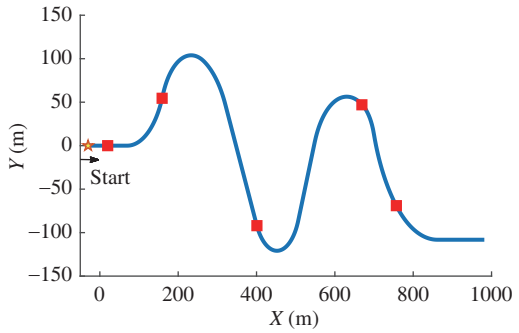

Figure 10 (Color online) The road used in the simulation study. The lane width is 3.5 m, and there are 5 slow-moving vehicles (represented by red rectangles) on the road, while the yellow star is the starting position.

Figure 11 (Color online) Simulation scenario of a rear-end collision avoidance. The black vehicle is the host vehicle and the blue truck is the front vehicle.

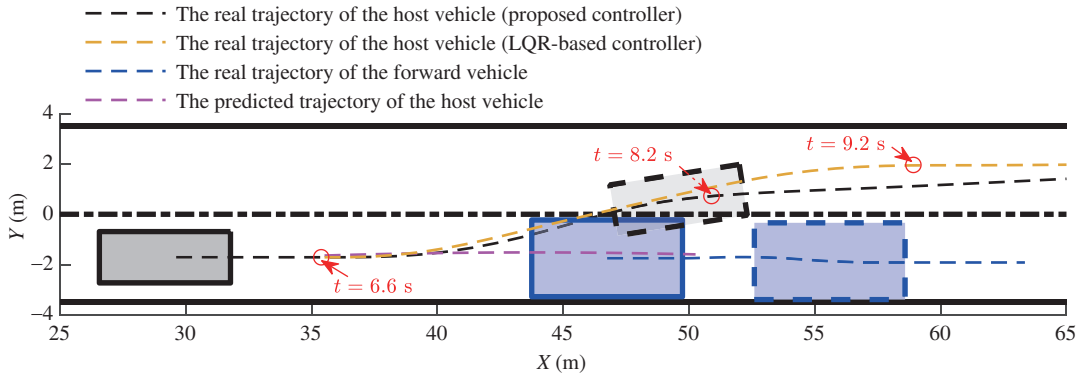

Figure 12 (Color online) The rear-end collision avoidance with the proposed controller and the LQR-based one. The dashed black and dashed blue rectangles depict the real states of the host and forward vehicles at the predicted collision time. $t = 6.6$ s is the triggering time instant, $t = 8.2$ s and $t = 9.2$ s correspond to the time instants when $\alpha \geqslant \bar{\alpha}$.

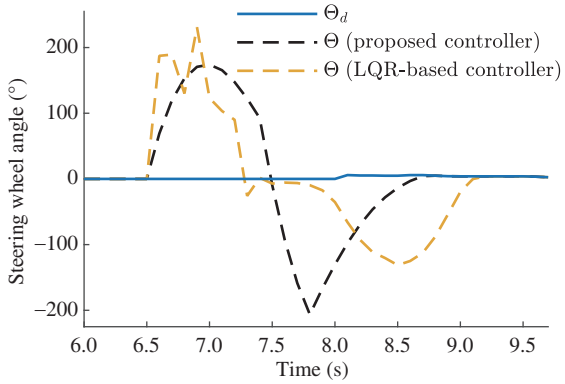

Figure 13 (Color online) The control variables of the rear-end collision avoidance with the proposed controller and the LQR-based one.

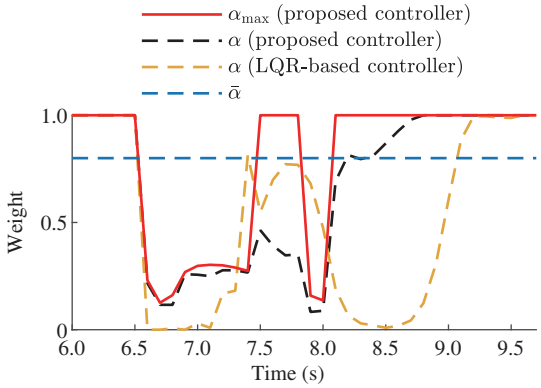

Figure 14 (Color online) The control shares of the driver during the rear-end collision avoidance with the proposed controller and the LQR-based one.

controller will be triggered to actively assist the driver in avoiding an imminent collision. As shown in Figure 12, when the simulation time reaches 6.6 s, the risk assessment module identifies the collision risk for the first time. Therefore, the shared controller starts to take action until the safety hazard is eliminated and the driver takes over the vehicle. The results show that both controllers can successfully avoid the potential rear-end collision. But the LQR-based controller takes more time to realize the switching condition $\alpha \geqslant \bar{\alpha}$.

The steering wheel angles contributed by the driver and the shared steering wheel angles in this rear-end collision avoidance process are shown in Figure 13. It can be seen that the curve of the shared steering wheel angles generated by the proposed controller is smoother. Figure 14 shows the change in

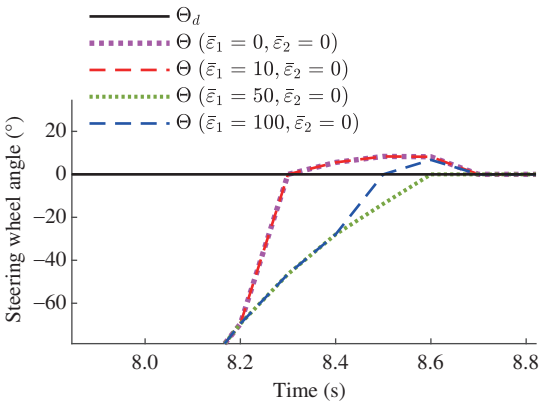

Figure 15 (Color online) The transitions of rear-end collision avoidance for $\bar{\varepsilon}_2 = 0$ with different $\bar{\varepsilon}_1$.

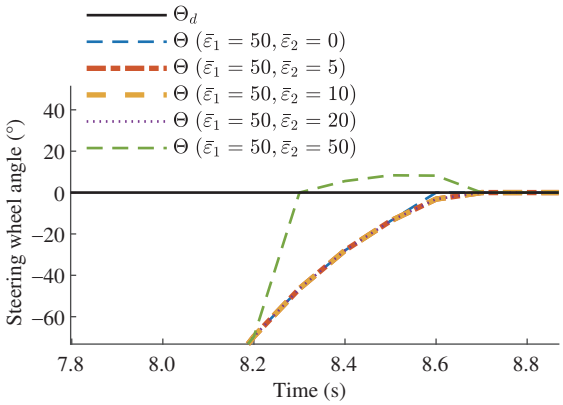

Figure 16 (Color online) The transitions of rear-end collision avoidance for $\bar{\varepsilon}_1 = 50$ with different $\bar{\varepsilon}_2$.

the driver's control share and its upper bound during this process. At the beginning of shared control with the proposed approach, i.e., $t = 6.6$ s, the value of the upper bound of α, i.e., $\alpha_{\max}$ drops rapidly owing to the increase of risk level. Then in the time interval $[7.4, 7.8]$ s, the driver behavior can support the lane change process. In this case, the risk assessment module confirms that the behavior of the driver can ensure the safety of the vehicle in the prediction horizon, and the upper bound of α is set to 1 again. Since the condition of the transition from shared control to human driving mode, $\alpha(t-i) \geqslant \bar{\alpha}$, for $i = 1, \ldots, r$, is not met, the shared control mode is still remained. At the simulation time $t = 8.2$ s, the safety hazard is reduced and the risk assessment module confirms that the driver behavior can guarantee the safe driving of the host vehicle, and the objective function (12) is to be used. When the host vehicle accomplishes collision avoidance, the value of α is approaching to 1 until the transition condition is met and the driver retrieves fully control authority again.

It can also be seen in Figure 14 that, the LQR-based controller behaves more aggressively than the proposed approach in the initial stage after the controller is triggered, i.e., in the time interval $[6.6, 6.8]$ s. The control share of the driver becomes almost zero, as the lateral error between the real trajectory and the desired path is reduced in the time interval $[7.3, 7.9]$ s, and the driver gains greater control share and the shared steering wheel angle is close to the driving behavior. At the time $t = 9.2$ s, the condition $\alpha \geqslant \bar{\alpha}$ is fulfilled, which is 1 s later than that with the proposed approach. Although the LQR-based controller can finally achieve a smooth transition to the human driving mode, the authority allocation strategy that depends on the tracking error is passive, which results in a longer intervention time period than that with the proposed approach.

To show how the values of $(\bar{\varepsilon}_1, \bar{\varepsilon}_2)$ affect the smooth transition, we also performed the simulations with the proposed approach using different values of $(\bar{\varepsilon}_1, \bar{\varepsilon}_2)$. As shown in Figure 15, it can be seen that for the case $\bar{\varepsilon}_2 = 0$, when $\bar{\varepsilon}_1 = 0, 10$, the variation of steering wheel angle reaches fast to zero, and then experiences a transient period of about 0.35 s. When it comes to the case that $\bar{\varepsilon}_1 = 50$, a smoother transition of the control action can be achieved. Keeping increasing the value of $\bar{\varepsilon}_1$ to 100 does not guarantee a better transition performance, and this might be because the penalty on β in this case is too large that it affects the overall control performance. To show that the penalty on the increment of β can help to achieve a much smoother transition, we also tested the algorithm for the case $\bar{\varepsilon}_1 = 50$ but with different choices of $\bar{\varepsilon}_2$. The results depicted in Figure 16 show that a much smoother transition from shared control to human driving mode can be achieved for the choices $\bar{\varepsilon}_2 = 5, 10, 20$, than that for the case $\bar{\varepsilon}_2 = 0$. However, $\bar{\varepsilon}_2 \geqslant 50$ is not advisable in this scenario.

6.3 Lane-departure avoidance

Extremely abnormal driving behaviors, that will cause a danger event, do exist, such as the driver unintentionally turning the steering wheel in the wrong direction, or a passenger trying to grab the steering wheel. This subsection considers a scenario where the host vehicle is about to enter a curve road from a straight one with a large force acting on the steering wheel, so the vehicle turns sharply in the opposite direction, as shown in Figure 17. We verified whether the risk assessment module can respond quickly and the shared lateral controller can correct the vehicle trajectory to keep in lane.

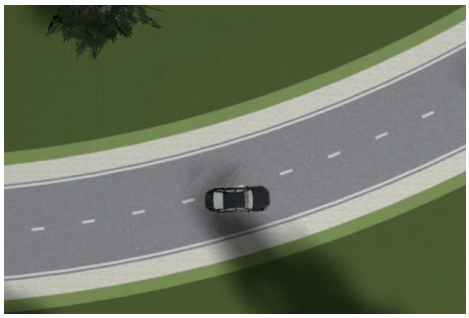

Figure 17 (Color online) Simulation scenario of the lane-departure avoidance. The black vehicle is going off the road.

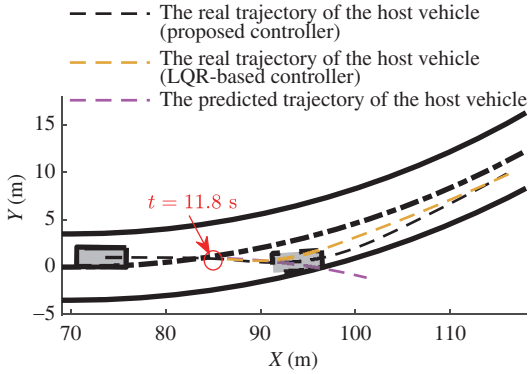

Figure 18 (Color online) The lane-departure avoidance. The dashed black rectangle depicts the real state of the host vehicle at the predicted collision time predicted in collision detection. $t = 11.8$ s is the triggering time instant.

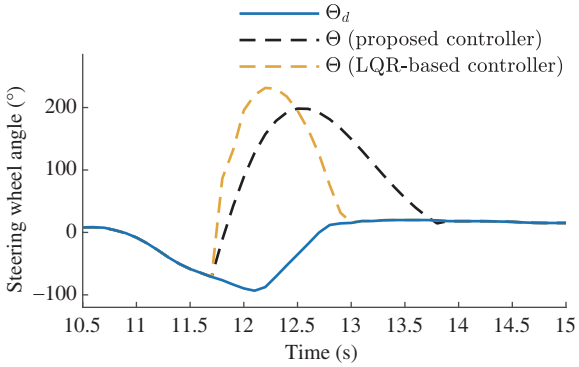

Figure 19 (Color online) The control variables of the lane-departure avoidance with the proposed controller and the LQR-based one.

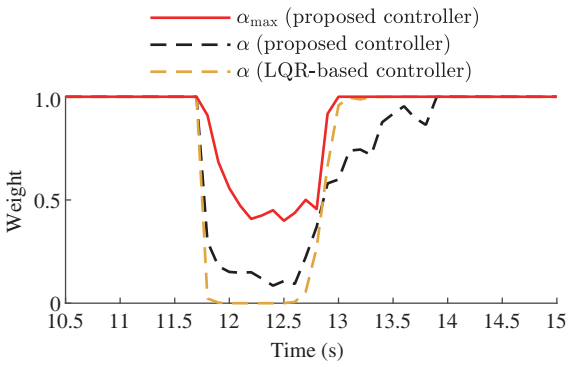

Figure 20 (Color online) The control shares of the driver during the lane-departure avoidance with the proposed controller and the LQR-based one.

As illustrated in Figure 18, at the simulation time $t = 11.8$ s, the risk assessment module recognizes the collision risk and the driving mode of the vehicle is transferred to shared control. The vehicle successfully avoids lane-departure in two experiments with both controllers. The driver's behaviors and the shared inputs to the steering-by-wire system during the lane-departure avoidance are shown in Figure 19. In the time interval $[10.7, 12.1]$ s, the driver takes a number of wrong actions, while in the last half time the driver's behaviors gradually return to normal. Compared with the LQR-based controller, the shared steering wheel angles generated by the proposed controller are smoother and the rate of change is smaller. The variations of α and $\alpha_{\max}$ are presented in Figure 20. The results show that the control authority returns back to the driver from the proposed controller at time $t = 13.8$ s, which is about 0.8 s after the time instant when $w < w_0$. Also, at the end of the shared control, the shared inputs gradually approach the driver's behaviors and a smooth transition to human driving mode is achieved. As for the LQR-based controller, the shared control policy and the transition back to the driver are more aggressive than that with the proposed one, which might cause excessive lateral acceleration of the vehicle and make the driver feel uncomfortable.

6.4 Collision avoidance for unskilled driving

In this simulation scenario, we tested whether the proposed shared control system can deal with the potential collisions owing to the insufficient steering torque which usually happens to unskilled drivers, as shown in Figure 21.

At simulation time $t = 23.4$ s, a collision risk is detected by the risk assessment module, and the risk is estimated to happen in 1.4 s later, as shown in Figure 22. The comparisons of simulation results between the proposed approach and the LQR-based controller are presented in Figures 23 and 24. Similar to that of the previous two simulation scenarios, when the intervention is over, the proposed approach can

Figure 21 (Color online) Simulation scenario of collision avoidance for unskilled driving on a curve road. The driver is unskilled to apply a sufficient torque on the steering wheel, so the host vehicle is crashing to the forward vehicle in the adjacent lane.

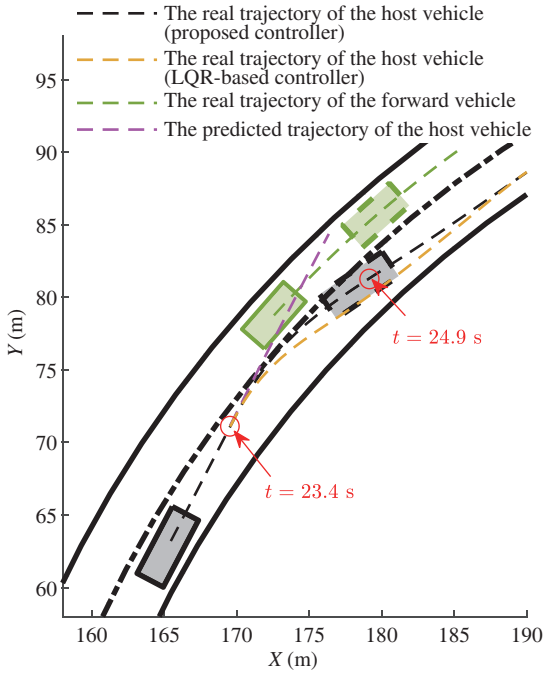

Figure 22 (Color online) The collision avoidance for unskilled driving. The dashed black and dashed green rectangles depict the real states of the host and forward vehicles at the collision time predicted in collision detection. $t = 23.4$ s is the triggering time instant, $t = 24.9$ s corresponds to the time instant when $\alpha \geqslant \bar{\alpha}$.

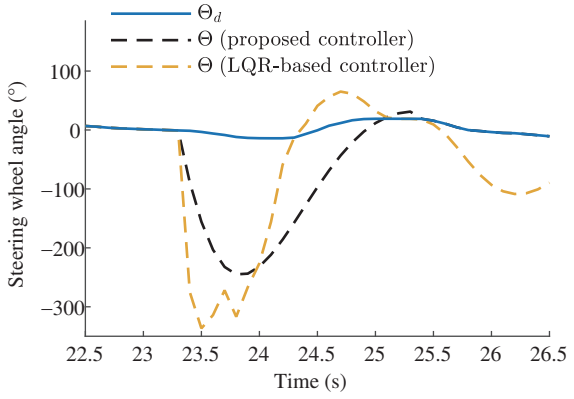

Figure 23 (Color online) The control variables of the collision avoidance for unskilled driving with the proposed controller and the LQR-based one.

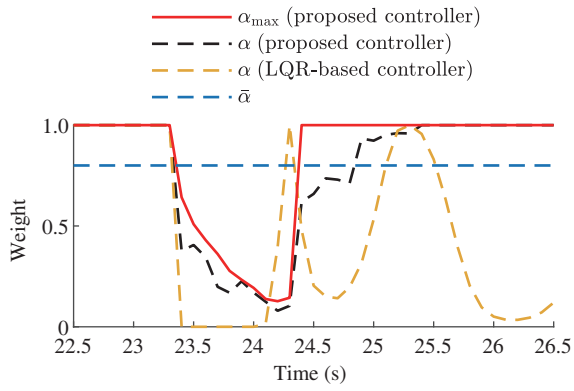

Figure 24 (Color online) The control shares of the driver during the collision avoidance for unskilled driving.

successfully switch back to the human driving mode smoothly. However, the LQR-based controller is failed in this respect, i.e., it cannot give the control authority back to human timely even if the danger has been passed. The reason behind is that its control share allocation strategy relies on the current lateral error, which makes the intervention easily happen again.

In addition, in order to show the real-time property of the proposed controller, we have collected the average computation time in the above three simulation scenarios, i.e., $t = 0.0236$ s, which is much smaller than the adopted sampling time interval $T = 0.1$ s. In fact, a shorter time interval $T = 0.025$ s is also applicable with the proposed controller.

7 Conclusion

In this paper, an event-triggered shared lateral controller has been proposed for collision-free maneuver. In view of its main characteristics, the online risk assessment can be realized by only predicting the trajectories of vehicles via a Bayesian regularized artificial neural network, no human driving intention information is required. With this choice, potential risks and the intervention time are properly determined. A safe-maneuver oriented shared lateral controller has been designed, where the control shares of the human and intelligent system are optimized continuously via solving an MPC problem. The future driver's behavior intention used in the optimization has been modeled as an online model predictor steering the predicted trajectories contributed by human driving. Also, the smooth transition issue from the shared control to human driving mode has been dealt with in the optimization problem. Comprehensive studies, including the comparison with an LQR-based shared controller, have been performed on a high-fidelity PreScan environment focusing on three typical scenarios. The results show that the proposed approach can detect the collision risks accurately and correct the control actions to avoid potential collisions timely. Moreover, the smooth transition back to human driving mode is realized and the control performance in this respect is better than the LQR-based controller. Future work will focus on the validation on a real vehicle platform and the use of ADP-based method for the shared control design with safety guarantees.

Acknowledgements The work was supported by National Natural Science Foundation of China (Grant Nos. 61751311, 61825305) and National Key R&D Program of China (Grant No. 2018YFB1305105).

References

1 Hu Y, Qu T, Liu J, et al. Human-machine cooperative control of intelligent vehicle: recent developments and future perspectives. Acta Automa Sin, 2019, 45: 1261–1280
2 Petermeijer S M, Abbink D A, de Winter J C F. Should drivers be operating within an automation-free bandwidth? Evaluating haptic steering support systems with different levels of authority. Human Factors, 2015, 57: 5–20
3 Hamid U Z A, Saito Y, Zamzuri H, et al. A review on threat assessment, path planning and path tracking strategies for collision avoidance systems of autonomous vehicles. Int J Veh Autonom Syst, 2018, 14: 134–169
4 Bengler K, Dietmayer K, Farber B, et al. Three decades of driver assistance systems: review and future perspectives. IEEE Intell Transport Syst Mag, 2014, 6: 6–22
5 Saito T, Wada T, Sonoda K. Control authority transfer method for automated-to-manual driving via a shared authority mode. IEEE Trans Intell Veh, 2018, 3: 198–207
6 Sentouh C, Debernard S, Popieul J C, et al. Toward a shared lateral control between driver and steering assist controller. IFAC Proc Vol, 2010, 43: 404–409
7 Ludwig J, Martin M, Horne M, et al. Driver observation and shared vehicle control: supporting the driver on the way back into the control loop. Automatisierungstechnik, 2018, 66: 146–159
8 Huang C, Naghdy F, Du H, et al. Shared control of highly automated vehicles using steer-by-wire systems. IEEE/CAA J Autom Sin, 2019, 6: 410–423
9 de Winter J C F, Happee R, Martens M H, et al. Effects of adaptive cruise control and highly automated driving on workload and situation awareness: a review of the empirical evidence. Transpation Res Part F-Traffic Psychol Behaviour, 2014, 27: 196–217
10 Borroni F, Tanelli M. A weighting approach to the shared-control of lateral vehicle dynamics. IFAC-PapersOnLine, 2018, 51: 305–310
11 Nguyen A T, Sentouh C, Popieul J C. Sensor reduction for driver-automation shared steering control via an adaptive authority allocation strategy. IEEE/ASME Trans Mechatron, 2018, 23: 5–16
12 Zafeiropoulos S, Tsiotras P. Design of a lane-tracking driver steering assist system and its interaction with a two-point visual driver model. In: Proceedings of the 2014 American Control Conference, Portland, 2014. 3911–3917
13 Merah A, Hartani K, Draou A. A new shared control for lane keeping and road departure prevention. Vehicle Syst Dyn, 2016, 54: 86–101
14 Jiang J, Astolfi A. State and output-feedback shared-control for a class of linear constrained systems. IEEE Trans Automat Contr, 2016, 61: 3209–3214
15 Jiang J, Astolfi A. Shared-control for a rear-wheel drive car: dynamic environments and disturbance rejection. IEEE Trans Human-Mach Syst, 2017, 47: 723–734
16 Jiang J, Astolfi A. Shared-control for the lateral motion of vehicles. In: Proceedings of the 2018 European Control Conference (ECC), Limassol, 2018. 225–230
17 Saleh L, Chevrel P, Claveau F, et al. Shared steering control between a driver and an automation: stability in the presence of driver behavior uncertainty. IEEE Trans Intell Transp Syst, 2013, 14: 974–983
18 Huang M, Gao W, Wang Y, et al. Data-driven shared steering control of semi-autonomous vehicles. IEEE Trans Human-Mach Syst, 2019, 49: 350–361
19 Park K, Han S H, Lee H. A study on shared steering control in driving experience perspective: how strong and how soon should intervention be? 2018. ArXiv: 1809.05869
20 Brandt T, Sattel T, Bohm M. Combining haptic human-machine interaction with predictive path planning for lane-keeping and collision avoidance systems. In: Proceedings of the 2007 IEEE Intelligent Vehicles Symposium, Istanbul, 2007. 582–587
21 Li R J, Li S B, Gao H B, et al. Effects of Human Adaptation and Trust on Shared Control for Driver-Automation Cooperative Driving. SAE Technical Paper, No. 2017-01-1987. 2017
22 Anderson S J, Peters S C, Pilutti T E, et al. An optimal-control-based framework for trajectory planning, threat assessment, and semi-autonomous control of passenger vehicles in hazard avoidance scenarios. Int J Veh Autonom Syst, 2010, 8: 190–216
23 Gray A, Ali M, Gao Y Q, et al. Semi-autonomous vehicle control for road departure and obstacle avoidance. In: Proceedings of the 2012 IFAC Symposium on Control in Transportation Systems, Sofia, 2012. 1–6

24 Wang Y L, Zheng H Y, Zong C F, et al. Path-following control of autonomous ground vehicles using triple-step model predictive control. Sci China Inf Sci, 2020, 63: 209203
25 Wu Y, Ren G P, Zhang H T. Dual-mode predictive control of a rotor suspension system. Sci China Inf Sci, 2020, 63: 112204
26 Li Y, Tee K P, Yan R, et al. Shared control of human and robot by approximate dynamic programming. In: Proceedings of the 2015 American Control Conference (ACC), Chicago, 2015. 1167–1172
27 Lee D N. A theory of visual control of braking based on information about time-to-collision. Perception, 1976, 5: 437–459
28 Zhang Y, Antonsson E K, Grote K. A new threat assessment measure for collision avoidance systems. In: Proceedings of the 2016 IEEE Intelligent Transportation Systems Conference, Toronto, 2006. 968–975
29 Brannstrom M, Coelingh E, Sjoberg J. Model-based threat assessment for avoiding arbitrary vehicle collisions. IEEE Trans Intell Transp Syst, 2010, 11: 658–669
30 Althoff M, Mergel A. Comparison of Markov chain abstraction and Monte Carlo simulation for the safety assessment of autonomous cars. IEEE Trans Intell Transp Syst, 2011, 12: 1237–1247
31 Anderson S J, Karumanchi S B, Iagnemma K. Constraint-based planning and control for safe, semi-autonomous operation of vehicles. In: Proceedings of the 2012 IEEE Intelligent Vehicles Symposium, Alcala de Henares, 2012. 383–388
32 Wada N, Matsumoto T. Driver assistance for collision avoidance by constrained MPC. In: Proceedings of the 2017 56th Annual Conference of the Society of Instrument and Control Engineers of Japan (SICE), Kanazawa, 2017. 90–93
33 Kitagawa L, Kobayashi T, Beppu T, et al. Semi-autonomous obstacle avoidance of omnidirectional wheelchair by joystick impedance control. In: Proceedings of the 2001 IEEE/RSJ International Conference on Intelligent Robots and Systems, Maui, 2001. 2148–2153
34 Itoh M, Tanaka H, Inagaki T. Toward trustworthy haptic assistance system for emergency avoidance of collision with pedestrian. J Human-Robot Interaction, 2015, 4: 4
35 Balachandran A, Brown M, Erlien S M, et al. Predictive haptic feedback for obstacle avoidance based on model predictive control. IEEE Trans Automat Sci Eng, 2016, 13: 26–31
36 Rajamani R. Vehicle Dynamics and Control. Berlin: Springer Science & Business Media, 2011
37 Gong J, Jiang Y, Xu W. Model Predictive Control for Self-driving Vehicles. Beijing: Beijing Institute of Technology Press, 2014
38 Martinez J, Black M J, Romero J. On human motion prediction using recurrent neural networks. In: Proceedings of the IEEE Conference on Computer Vision and Pattern Recognition, Hawaii, 2017. 2891–2900
39 Lefèvre S, Vasquez D, Laugier C. A survey on motion prediction and risk assessment for intelligent vehicles. ROBOMECH J, 2014, 1: 1–14
40 Kim B D, Kang C M, Kim J, et al. Probabilistic vehicle trajectory prediction over occupancy grid map via recurrent neural network. In: Proceedings of 2017 IEEE 20th International Conference on Intelligent Transportation Systems, Yokohama, 2017. 399–404
41 Agamennoni G, Nieto J I, Nebot E M. Estimation of multivehicle dynamics by considering contextual information. IEEE Trans Robot, 2012, 28: 855–870
42 MacKay D J C. Bayesian interpolation. Neural Comput, 1992, 4: 415–447
43 Ticknor J L. A Bayesian regularized artificial neural network for stock market forecasting. Expert Syst Appl, 2013, 40: 5501–5506
44 Sun Z, Chen Y, Li X, et al. A Bayesian regularized artificial neural network for adaptive optics forecasting. Opt Commun, 2017, 382: 519–527
45 Foresee F D, Hagan M T. Gauss-Newton approximation to Bayesian learning. In: Proceedings of International Conference on Neural Networks (ICNN'97), Houston, 1997. 1930–1935
46 Ercan Z, Carvalho A, Tseng H E, et al. A predictive control framework for torque-based steering assistance to improve safety in highway driving. Vehicle Syst Dyn, 2018, 56: 810–831
47 Chen H, Allgöwer F. A quasi-infinite horizon nonlinear model predictive control scheme with guaranteed stability. Automatica, 1998, 34: 1205–1217
48 Chmielewski D, Manousiouthakis V. On constrained infinite-time linear quadratic optimal control. Syst Control Lett, 1996, 29: 121–129